Since January 2020 Elsevier has created a COVID-19 resource centre with free information in English and Mandarin on the novel coronavirus COVID-19. The COVID-19 resource centre is hosted on Elsevier Connect, the company's public news and information website.

Bone 83 (2016) 190–196

Contents lists available at ScienceDirect

Bone

journal homepage: www.elsevier.com/locate/bone

Original Full Length Article

Src siRNA prevents corticosteroid-associated osteoporosis in a rabbit model

Li-Zhen Zheng [a], Xin-Luan Wang [a,b], Hui-Juan Cao [b], Shi-Hui Chen [a], Le Huang [a], Ling Qin [a,b,*]

[a] Musculoskeletal Research Laboratory, Department of Orthopaedics & Traumatology, The Chinese University of Hong Kong, Hong Kong, China
[b] Translational Medicine R&D Center, Institute of Biomedical and Health Engineering, Shenzhen Institutes of Advanced Technology, Chinese Academy of Sciences, Shenzhen, PR China

ARTICLE INFO

Article history:
Received 24 July 2015
Revised 13 November 2015
Accepted 16 November 2015
Available online 18 November 2015

Keywords:
Src
siRNA
Osteoporosis
Corticosteroid

ABSTRACT

In an established steroid-associated osteonecrosis (SAON) rabbit model we found recently that blockage Src by siRNA could improve reconstructive repair of osteonecrosis *via* enhancing osteogenesis and inhibiting bone resorption. The current study investigated if blocking Src was able to prevent steroid-associated osteoporosis (SAOP) in the same SAON animal model. Rabbits were treated with pulsed lipopolysaccharide (LPS) and corticosteroid methylprednisolone (MPS). At 2, 4, and 6 weeks after induction, Src siRNA, control siRNA and saline were intramedullary injected into proximal femur, respectively. Two fluorescent dyes xylenol orange and calcein green were injected before sacrificing the animals for *in vivo* labeling of the newly formed bone. At week 6 after induction, proximal femora of rabbits were dissected for micro-CT and histological analysis. Results showed significant bone loss in the metaphysis of femoral head in the control rabbits after SAON induction. Src siRNA treatment was able to prevent steroid-associate bone loss in trabecular bone and increase cortical bone thickness at femoral neck. Histomorphometry showed that Src siRNA increased the osteoblastic bone formation and decreased the eroded bone surfaces suggesting decreased osteoclastic bone resorption. This was the first study to report bone loss after SAON induction in rabbit model that could be prevented by knocking down Src by siRNA.

1. Introduction

Corticosteroids are widely indicated for many diseases attributed to its anti-inflammation effects. However, its long-term use could lead to adverse effects such as steroid-associated osteoporosis (SAOP) [1] and/or steroid-associated osteonecrosis (SAON) [2]. SAOP patients with decreased bone mineral density (BMD) are reported at higher risk of bone fracture [3] and the advanced SAON patients often suffered from joint collapse [4]. Physiologically, the skeleton undergoes remodeling, with osteoclasts for resorbing old bone and osteoblasts for forming new bone towards maintenance of bone homeostasis [5]. Corticosteroids impair osteoblastic osteogenesis and increase apoptosis of osteoblasts and osteocytes. This has been regarded as common pathway or the underlying mechanism of corticosteroids-associated bone deterioration in both SAOP and SAON [6].

Proto-oncogene tyrosine-protein kinase Src (also known as c-Src) participates in regulating a wide range of cell functions, including adhesion, motility, proliferation and survival [7,8]. In skeletal system, Src inhibits osteoblast differentiation [9]. It is reported that the decreased Src expression enhances osteoblast differentiation and bone formation [10]. Src is also involved in regulating osteoclastic bone resorption [11] as it is essential for the function of osteoclasts *via* regulating the osteoclast skeleton [12]. Transgenic expression of Src can also rescue osteoclast function in Src knockout mice [13].

In a modified SAON rabbit model, we found destructive repair at subchondral region of femoral head, *i.e.* a dominate old bone resorption without adequate new bone formation to maintain normal bone homeostasis; and knockdown of Src expression by Src specific siRNA could enhance osteoblast differentiation, promote osteogenesis and inhibit the function of osteoclasts [14]. In other words, Src siRNA may also have potential for treatment of SAOP. In this study, we investigated corticosteroid-associated bone loss at metaphysis of femoral head using an established SAON rabbit model [14] and potential effects of Src siRNA for prevention of SAOP.

2. Material and methods

2.1. Animals and steroid induction

Forty-eight 28-week-old male New-Zealand white rabbits (4.0 ± 0.5 kg) were housed at the Experimental Animal Center in Prince of Wales Hospital in Hong Kong and received a standard laboratory diet and water *ad libitum*. All specified experimental protocols were approved by the Animal Experiment Ethics Committee of the Chinese University of Hong Kong (11/029/GRF).

* Corresponding author at: Rm74026, 5/F, Clinical Science Building, Prince of Wales Hospital, Shatin, Hong Kong, China.
E-mail address: lingqin@cuhk.edu.hk (L. Qin).

http://dx.doi.org/10.1016/j.bone.2015.11.010
8756-3282/

Based on our established protocol for inducing destructive repair SAON, thirty-six rabbits were used and intravenously injected with lipopolysaccharide (LPS) (10 μg/kg body weight, Escherichia coli O111:B4; Sigma-Aldrich, St. Louis, MO, USA) on day 0 and day 14, and intramuscularly injected with corticosteroid methylprednisolone (MPS) (20 mg/kg body weight, Pharmacia & Upjohn, Peapack, NJ, USA) on days 1, 2, 3 and again on days 15, 16 and 17 [14]. Twelve rabbits without any treatment were used as normal controls.

2.2. siRNA administration

At 2, 4 and 6 weeks after induction with pulsed LPS and MPS, rabbits were under general anesthesia with intramuscular injection of xylazine (20 mg/kg body weight) and ketamine (50 mg/kg body weight) for hair shaving on hip region and prepped with iodine tincture and 70% ethanol. Lateral digital x-ray of hip was taken for monitoring the injection site. In order to prove the intervention concept, we adopted local delivery approach where a 19 G needle was selected for local siRNA administration and for controls as well by inserting it from the greater trochanter of proximal femur to the marrow cavity of the femur neck.

The LPS-MPS treated rabbits were randomly divided into three groups (n = 12/group): 1) S-siSrc Group: 5 nmol Src siRNA (synthesized by RiboBio, Guangzhou RiboBio Co., Ltd., sense 5′-GGU UCA CCA UCA AGU CAG A dTdT-3′, antisense 5′-UCU GAC UUG AUG GUG AAC C dTdT-3′) was intramedullary injected into each proximal femur with 10 μl *in vivo*-jetPEI (PolyPlus Transfection, Strasbourg, France) as transfection reagent according to the manufactural protocol; 2) S-NC group: 5 nmol negative control siRNA (synthesized by RiboBio, sense 5′-UUC UCC GAA CGU GUC ACG U dTdT-3′, antisense 5′-ACG UGA CAC GUU CGG AGA A dTdT-3′.) was injected with the same method described above; and 3) S-VC group: Vehicle control (0.5 ml saline) was injected. Euthanasia was executed 4 days after the week 6 administration for each group and the femora were collected for further evaluations.

2.3. Quantitative PCR

0.2 ml bone marrow was extracted from the injection site before injection for mRNA isolation with RNeasy® Mini Kit (Qiagen, USA) and then cDNA was reverse transcripted by QuantiTect® Reverse Transcription Kit (Qiagen, USA). Real-time PCR was performed by ABI Prism 7700 sequence Detection System (Applied Biosystem, Foster City, CA, USA) using TF pack power SYBR Green PCR Mas (Applied Biosystem, Foster City, CA, USA). Primers for rabbit are:

Src-forward 5′-GCCCATCTACATCGTCACAG-3′,
Src-reverse 5′-TAGTTCATCCGCTCCACGTA-3′,
GAPDH-forward 5′-TCTGGCAAAGTGGATGTTGT-3′,
GAPDH-reverse 5′-GTGGGTGGAATCATACTGGA-3′.

2.4. Sequential fluorescence labeling

At day 14 and day 7 before euthanasia, two fluorescent dyes, xylenol orange (90 mg/kg body weight) and calcein green (10 mg/kg body weight; both Sigma-Aldrich GmbH), were injected sequentially and subcutaneously into the rabbits (n = 4/group). After euthanasia, the proximal femora were embedded in methyl methacrylate (MMA) without decalcification.

2.5. Micro-CT scanning and analysis

After being fixed in buffered formalin for one week, the proximal femora were scanned using a micro-CT (μCT-40, Scanco Medical, Brüttisellen, Switzerland) with a spatial resolution of 30 μm. In order to separate mineralized tissue from background signal, a low-pass Gaussian filter (Sigma = 0.8, Support = 1) was used. The mineralized tissue was defined at a threshold of 220 HU [15]. 2-D sections of the scanned femoral heads were then reconstructed into 3-D structure. To evaluate metaphyseal trabecular architecture of femoral head, a predetermined bone cylinder was used as ROI (3.5 mm diameter and 1.5 mm height) to quantify the volumetric bone mineral density (BMD), bone tissue volume fraction (BV/TV), connective density (Conn. D.), trabecular number (Tb. N), trabecular thickness (Tb.Th), and trabecular separation (Tb. Sp) [16]. To evaluate cortical bone, femoral neck was used as ROI (0.6 mm thick) after re-alignment of micro-CT images using built-in software IPL (Image Processing Language) (Fig. 3A). A dual threshold technique was used for automatic segmentation of cortical ring of the femoral neck [17]. The first threshold for outer contour and the second threshold for inner contour were both set at 220 HU. Using the micro-CT built-in evaluation methods for long bone midshaft evaluation, the cortical bone thickness (Ct.Th), periosteal diameter (Ps.Dm), endosteal diameter (Es.Dm) and polar moment of inertia (pMOI) were determined. The pMOI = Ixx + Iyy, where Ixx is MOI around x-axis, and Iyy is MOI around y-axis.

2.6. Histological and histomorphometric analysis

For decalcified sections, the proximal femora were treated with 10% EDTA (pH 7.4) for 8 weeks with weekly refreshing of the decalcifying solution (n = 8/group). The decalcification process was assessed by digital X-ray that the complete decalcification was confirmed without showing radiographic opacity. Then the proximal femora were embedded in paraffin and cut into 5-μm-thick sections along the coronal plane. Sections were stained with H&E for histomorphometry and tartrate-resistant acid phosphatase (TRAP, Sigma Diagnostics, St. Louis, Missouri, USA) for identification of osteoclasts.

The MMA embedded samples were cut along the coronal plane using a saw microtome (Leica SP1600, Leica Instruments, Nussloch, Germany) and polished to 100 μm by a polisher (Phoenix 4000, Buehler Ltd. USA) for observation of fluorescence labeling and then cut into 5-μm-thick sections using microtone (Leica RM2255) for dynamic histomorphometry and Goldner's trichrome staining.

Histological images were digitalized with a microscopic imaging system (Leica DM5500; Leica Micro-systems, Wetzlar, Germany). Histomorphometric analysis was carried out on the metaphysis of femoral head in a 3 mm width area below the growth plate by using OsteoMeasure Histomorphometry System (Osteometrics, Atlanta, GA, USA) and analyzed according to a standard histomorphometry protocol [18]. The osteoblast surface (ObS/BS), eroded surface (ES/BS), and the osteoclast number (N.Oc/BS and N.Oc/ES) were determined on the decalcified sections. The mineral apposition rate (MAR), mineralizing surface (MS/BS), bone formation rate (BFR/BS), and osteoid thickness (O.Wi) were determined on the un-decalcified sections. The MS = dLS + 0.5sLS, where dLS = double-label surface, sLS = single-label surface. BS = total bone surface. MAR = inter-label width/time between injection. BFR/BS = MAR × MS/BS [18].

2.7. Statistical analysis

All data were expressed as mean ± SD with one-way ANOVA followed by Bonferroni post-test to compare group differences. Statistical analysis was performed using SPSS 17.0 software (Chicago, IL, USA). $p < 0.05$ was considered significant.

3. Results

3.1. The efficiency of Src silencing in vivo

Quantitative real-time PCR showed that the Src mRNA level in bone marrow in S-siSrc group was consistently lower after week 2 injection compared to that of the S-NC group throughout the experimental period ($p < 0.05$), while the Src mRNA level in bone marrow in S-NC was not different when compared to that of the S-VC group (Fig. 1).

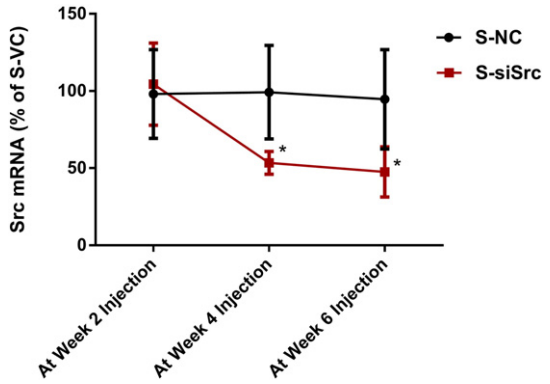

Fig. 1. The efficiency of Src silencing *in vivo*. Quantitative real-time PCR showed that the Src mRNA level in bone marrow of the S-siSrc group was consistently lower after week 2 injection compared to that of the S-NC group throughout the experimental period, while the Src mRNA level in bone marrow of the S-NC group was not different when compared to that of the S-VC group. (*: $p < 0.05$ compared to S-NC, $n = 6$).

3.2. Micro-CT-based quantification of trabecular architecture

We used micro-CT to analyze the metaphyseal trabecular architecture of femoral head. It revealed significant lower bone tissue volume fraction (BV/TV), trabecular thickness (Tb.Th) and connective density (Conn. D.) in S-VC/S-NC group when compared to those of the normal control group ($p < 0.05$ for all). On the contrary, metaphyseal trabecular bone showed significant higher bone mineral density (BMD) ($p < 0.05$), BV/TV ($p < 0.01$), Tb.Th ($p < 0.05$) and Conn. D. ($p < 0.05$) in S-siSrc group when compared to those of the S-VC/S-NC group. There was no significantly difference in each of above micro-CT parameters between S-VC and S-NC group (Fig. 2).

3.3. Micro-CT-based cortical bone evaluation

Micro-CT images of femoral neck showed that cortical thinning occurred in the S-VC group and S-NC group at the regions adjacent to greater trochanter and lesser trochanter when compared to the corresponding regions in the normal control group; and some thinning regions were even disconnected in the region adjacent to the greater trochanter (Fig. 3AB), while the average thickness of the whole ring cortical bone of the femoral neck (Ct.Th) did not show statistically significantly different between the S-VC/S-NC group and the normal control group. The Ct.Th and polar moment of inertia (pMOI) were significantly larger in the S-siSrc group when compared to those in the S-VC/S-NC group ($p < 0.05$). The periosteal diameter (Ps.Dm) and endosteal diameter (Es.Dm) were not significantly different among groups. (Fig. 3C).

3.4. Histomorphometry

Histomorphometric analysis was performed at the metaphysis of femoral heads (Fig. 4). From the decalcified sections, we found that the osteoblast surface (ObS/BS) of the S-VC/S-NC group was not different from that in the normal control group, while the ratio of eroded surface to total bone surface (ES/BS), and the osteoclast number per bone surface (N.Oc/BS) were significantly larger after induction when

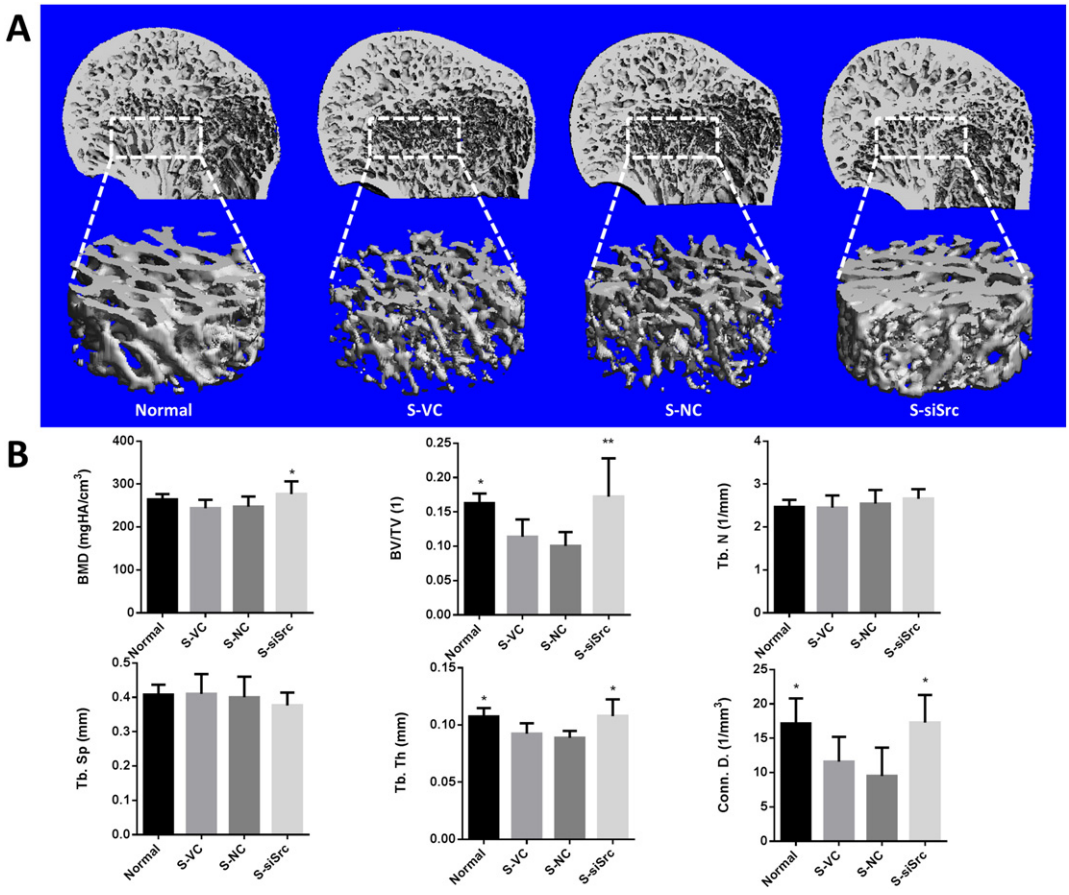

Fig. 2. Micro-CT-based trabecular architecture. (A) Representative 3D structure of femoral head of each group (upper layer) and metaphyseal trabecular architecture in femoral head region (lower layer) 6 weeks after pulsed LPS and MPS induction. (B) Quantitative analysis revealed a significant lower BV/TV, Tb. Th and Conn. D. in the S-VC/S-NC group when compared to those of the normal control group, and significant higher BMD, BV/TV, Tb.Th and Conn. D. in the S-siSrc group when compared to those of the S-VC/S-NC group. There was no significantly difference in above micro-CT parameters between the S-VC and the S-NC group. (*: $p < 0.05$,**: $p < 0.01$ compared to S-VC/S-NC group, $n = 8$ for each group).

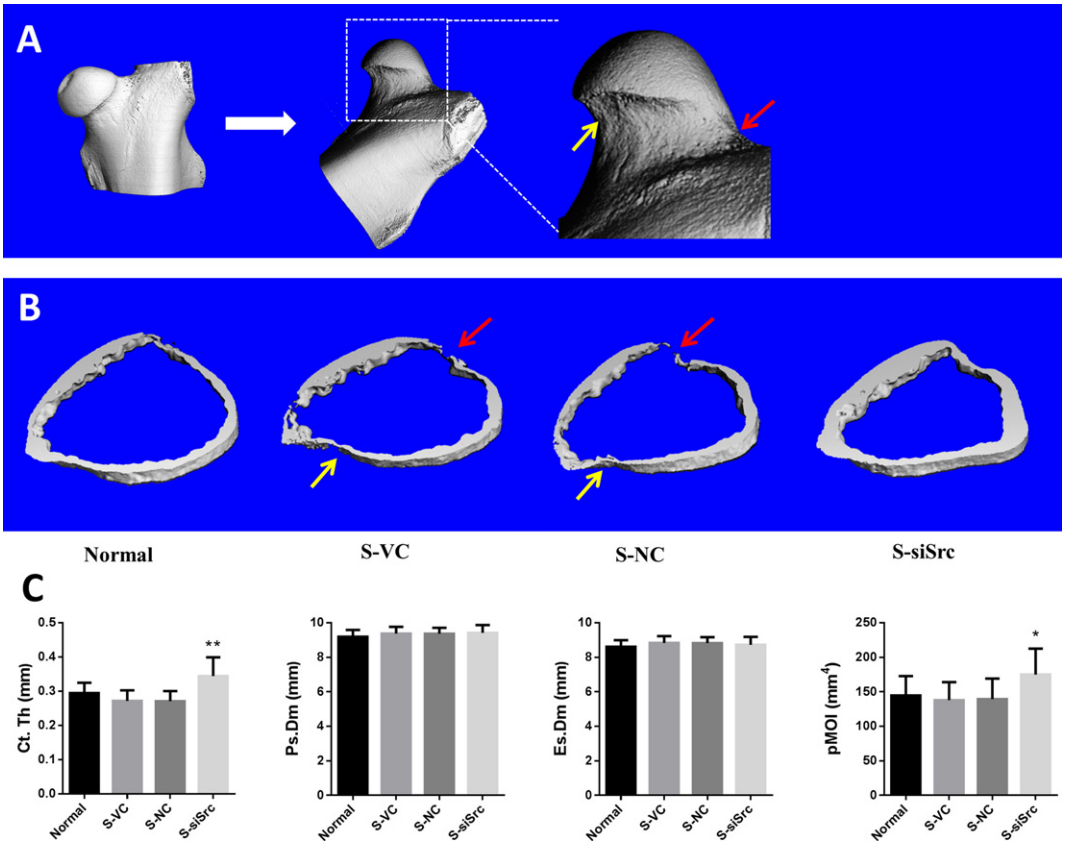

Fig. 3. Micro-CT-based cortical bone evaluation. (A) Re-alignment of 3D images for analysis of femoral neck. Arrows pointed corresponding cortical thinning (yellow arrows, adjacent to lesser trochanter) and dis-connected regions (red arrows, adjacent to greater trochanter) in the S-VC group and S-NC group. (B) Representative 3D images of femoral neck showed cortical thinning (yellow arrows) and even dis-connected regions (red arrows) in the S-VC group and the S-NC group. (C) Quantitative analysis revealed that the Ct.Th and pMOI were significantly larger in the S-siSrc group when compared to those of the S-VC/S-NC group. (*: $p < 0.05$, **: $p < 0.01$ compared to S-VC/S-NC group, $n = 8$ for each group).

compared to those in the normal group ($p < 0.05$). Src siRNA treatment significantly increased the ObS/BS while significantly decreased the ES/BS in S-siSrc group when compared to those in the S-VC/S-NC group ($p < 0.01$, Fig. 4). There was no significant difference in N.Oc/BS between S-siSrc group and S-VC/S-NC group, while the N.Oc/ES value was significantly larger in S-siSrc group when compared to that in the S-VC group ($p < 0.01$, Fig. 4). From the undecalcified sections, the results showed that in the S-VC/S-NC group the mineral apposition rate (MAR) and osteoid thickness (O.Wi) were lower when compared to those in the normal control group ($p < 0.01$), while the mineralizing surface (MS/BS) did not show significant difference. The bone formation rate (BFR/BS) was significantly lower in the S-VC/S-NC group when compared to that in the normal control group ($p < 0.05$). Src siRNA treatment did not affect the MAR and O.Wi when compared to those in the S-VC/S-NC group, while the MS/BS and the BFR/BS were significantly higher in S-siSrc group when compared to those of the S-VC/S-NC group ($p < 0.05$, Fig. 5).

3.5. Descriptive histology

Descriptive histological analysis on the femoral neck was summarized in Supplemental Fig. 1. The sequential fluorescence labeling showed newly formed bone on endosteal surface, including endocortical, intracortical, and trabecular surface, where we observed very little and scattered newly formed bone on periosteal surface at femoral neck in all the groups (Supplemental Fig. 1A). Goldner's trichrome staining showed some osteoid on the endocortical and intracortical surface in the normal control group and S-siSrc group. There was osteoclastic bone resorption in the S-VC and S-NC group, while in the S-siSrc group the osteoclastic bone resorption was hardly observed (Supplemental Fig. 1B).

4. Discussion

This study investigated the bone loss induced by pulsed LPS and MPS using an established SAON rabbit model and tested the therapeutic potential of Src siRNA, a bone anabolic and anti-resorption agent for prevention of corticosteroid associated osteoporosis (SAOP).

Our micro-CT analysis showed significant deterioration of trabecular bone at metaphysis of femoral head after LPS-MPS induction when compared with the normal control group, characterized with significant inferior values in BV/TV, Tb. Th and Conn. D. of the metaphysical trabecular bone of the femoral head in the S-VC/S-NC group. The histomorphometry results showed that the bone loss was explained by the increased osteoclastic bone resorption with increased osteoclast number (N.Oc/BS) and eroded surface, while with decreased osteoblastic bone formation accompanied by a decreased mineral apposition rate (MAR) and bone formation rate (BFR/BS). It is well-known that corticosteroid induces bone resorption [19,20], while long-term administration of corticosteroid would lead to the inhibition of osteoclastic bone resorption and reducing of bone turnover [21]. Our induction protocol with pulsed high dose of corticosteroid administration simulated the clinical situation, such as the one developed for treatment of severe acute respiratory syndrome (SARS) patients in Hong Kong in 2003 that resulted in lower BMD at the hip of SAON patients [22,23], while around the osteonecrotic lesions the osteoclasts were also stimulated to resorb necrotic trabecular bone in the repair process [24]. In this study, we investigated corticosteroid-associated bone loss using an established SAON rabbit model [14]. We found co-exist of osteonecrosis

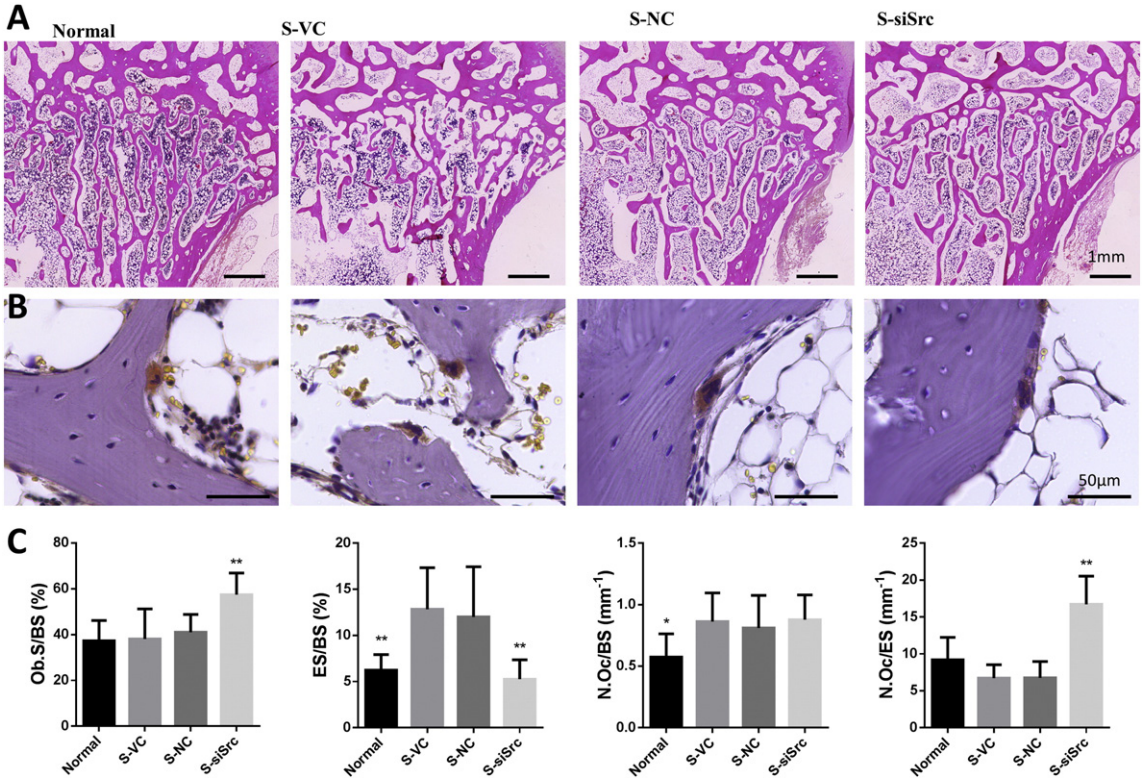

Fig. 4. Histomorphometric analysis on the decalcified sections. (A) H&E staining of the metaphysis of femoral head (auto-merged ×100 images). (B) TRAP staining showed the osteoclasts (×400). (C) Quantitative analysis of the osteoblast surface (ObS/BS), the ratio of eroded surface to total bone surface (ES/BS), the osteoclast number per bone surface (N.Oc/BS) and the osteoclast number per eroded surface (N.Oc/ES). (*: $p < 0.05$, **: $p < 0.01$ compared to S-VC/S-NC group, $n = 8$ for each group).

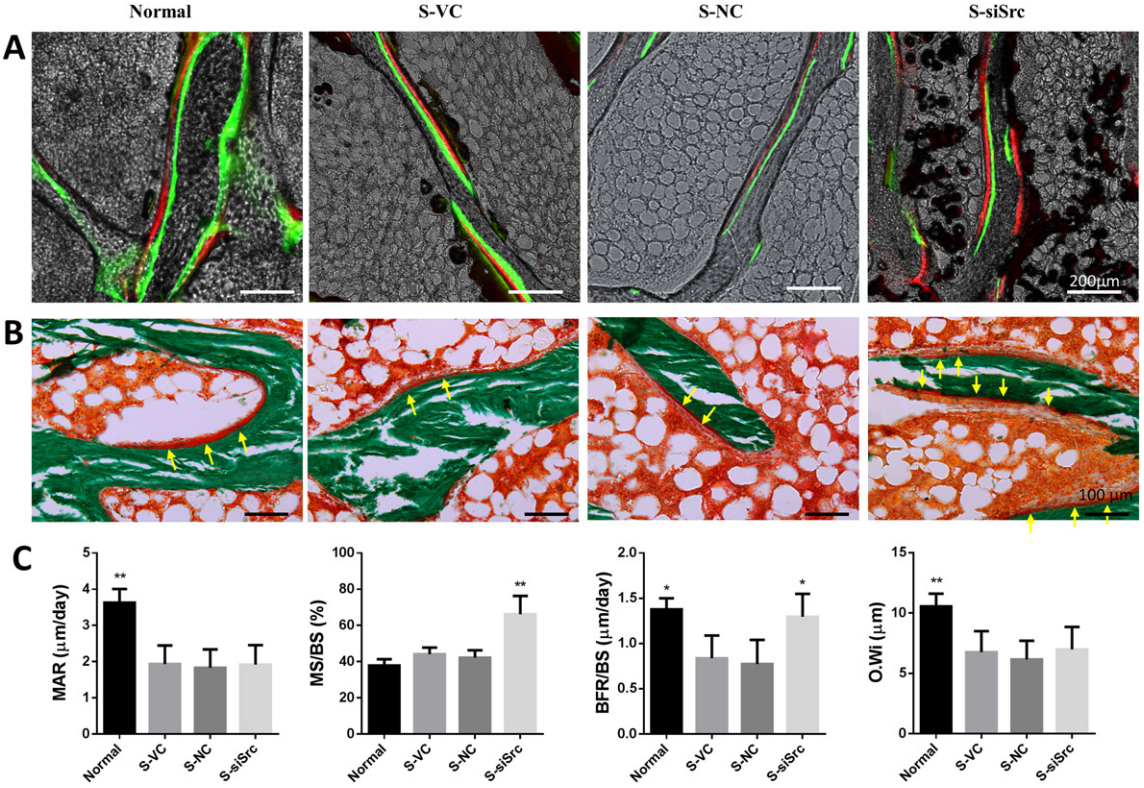

Fig. 5. Histomorphometric analysis on the undecalcified sections. (A) Sequential fluorescence labeling (auto-merged ×50 images). (B) Goldner's trichrome staining showed osteoids (yellow arrows) (×200 images). (C) Quantitative analysis of the mineral apposition rate (MAR), the mineralizing surface (MS/BS), the bone formation rate (BFR/BS) and the osteoid thickness (O.Wi). (*: $p < 0.05$, **: $p < 0.01$ compared to S-VC/S-NC group, $n = 4$ for each group).

and osteoporosis in the same animal model. However, the ROIs of osteonecrosis and osteoporosis were different and this made our evaluation possible for comparison. The subchondral region, where with yellow bone marrow and low bone remodeling rate in normal rabbit but with elevated bone resorption and bone formation in model animal, was the ROI for studying the repair of osteonecrosis; while the metaphysis, where with red bone marrow and normal bone remodeling, was the ROI for assessing bone loss associated with corticosteroid treatment in the current study. Although the apoptosis of osteoblasts and osteocytes induced by pulsed LPS and MPS inevitably occurred, it has been regarded as common pathway or the underlying mechanism of corticosteroids-associated bone deterioration in both SAOP and SAON [6]. This formed a structural basis for our novel findings of Src siRNA in prevention of SAOP. In the current study the pulsed LPS and MPS treatment down-regulated the metabolic activity of osteoblasts, as shown by a decreased MAR in S-VC/S-NC group. Similar findings were also reported in previous studies of SAOP [25,26]. However, the osteoblast surface (Ob.S/BS) and the mineralizing surface (MS/BS) were not significantly different between the S-VC and the normal control. This inconsistence might be explained that there was osteonecrotic repair progress in our animal model while purely SAOP had decreased osteoblast differentiation and proliferation [4,21,27–29]. Micro-CT images of femoral neck showed cortical thinning after the pulsed LPS-MPS treatment when compared with the normal control group at particular regions adjacent to greater trochanter and lesser trochanter, where cortical thickness was originally thinner and comparable to trabecular bone thickness to make these regions more sensitive to LPS-MPS. The overall changes in cortical thickness between were not found statistically significant that might be explained by rather short effects on cortical bone using our current pulsed MPS and LPS treatment protocol.

With regard to the SAON and SAOP, apart from MPS, LPS was also administered in our rabbit model to simulate clinical indication for treatment systemic inflammation [15]. It was reported that LPS could inhibit osteoblast differentiation and induce osteoblast apoptosis [30,31], and could promote osteoclast differentiation and survival [32], suggesting that LPS had potential contribution to the pathogenesis of the bone loss in our rabbit model as well, although we could not delineate its effects from corticosteroid. It was also reported that LPS could induce Src expression and activation in macrophages [33], *i.e.* the lineage of osteoclasts, for their potential contribution to activating of bone resorption.

The loss of trabecular bone at metaphysis of femoral head after pulsed LPS and MPS treatment was reversed by Src siRNA administration in the present study, with significantly better micro-CT indices, including BMD, BV/TV, Tb. Th and Conn. D. Our histomorphometry results confirmed that after Src siRNA administration, the Ob.S/BS, MS/BS and BFR/BS were significantly higher, suggesting that siSrc could enhance osteoblast differentiation in rabbit model. However, the MAR and O.Wi in S-siSrc group were not different from that in the S-VC/S-NC group, implying that siSrc did not affect the function of the mature osteoblasts. This finding was also supported by an early work using Src knockdown mice *in vivo* [10]. It was reported that inhibition of Src in calvarial osteoblasts from mice *in vitro* could lead to enhanced ALP activity and nodule mineralization, and the enhanced ALP activity was related to the enhanced ALP positive cell numbers [10]. It is known that Src family inhibits osteoblasts through Src-YAP-Runx2 signaling pathway by tyrosine phosphorylation of yes-associated protein (YAP) and then suppressing Runx2 transcriptional activity [34], where Runx2 is the major transcription factor controlling osteoblastogenesis [35]. It was reported that Src stimulated IL-6 and then induced insulin-like growth factor 5 (IGFBP5), a Src activating factor only in immature osteoblasts to maintain osteoblasts in a less mature status. This suggested that there could be different pathways of Src in regulating immature and mature osteoblasts, and this might be the reason of inhibiting Src stimulated osteoblast differentiation and maturity but without stimulating osteoblast function [9]. In the present study, we found N.Oc/BS was not affected by siSrc, suggesting that Src had no direct effect on the osteoclast differentiation; however, siSrc significantly decreased ES/BS and increased N. Oc/ES, suggesting that siSrc could inhibit osteoclastic bone resorption by inhibiting the bone resorption function of the osteoclasts. Higher N. Oc/ES means that if no change of the number of osteoclasts (N.Oc), the eroded surface (ES) is lower, or interpreted by lower average activity of osteoclasts. The function of Src in osteoclasts was its role in regulation of cytoskeletal organization [12], and organized cytoskeleton in osteoclast showed its effect on synthesis and secretion of collagenolytic cysteine proteases, such as Cathepsin K, while inhibition of Src was reported to suppress the secretion of cathepsins and bone resorption in osteoclasts [36], implying Src's involvement in activating bone resorption as well. It was reported that the lifespan of osteoclasts is about 2 weeks *in vivo*, and the lifespan will be longer with glucocorticoid excess [37]. This explained that the biweekly treatment with siRNA should have sustaining therapeutic effects on osteoclastic bone resorption.

In our current study, we also found that siSrc could enhance cortical bone thickness and the polar moment of inertia (pMOI), an indicator of torsional rigidity. Micro-CT revealed that the femoral neck cortical thickness in S-siSrc group was significantly increased compared with that in the S-VC/S-NC group. Clinically, the BMD measurement at the femoral neck is a standardized measurement to diagnose osteoporosis [38], and it is found that pMOI is also correlated to bone strength apart from BMD [39]. The bone fractures occurred predominantly at cortical sites, so the quality of cortical bone at femoral neck played an important role to predict the fracture risk [40]. Our fluorescence labeling showed new bone formation on the endocortical surface and intracortical surface (Supplemental Fig. 1). On the endosteal surface, including endocortical, intracortical, and trabecular surface, cells communicated in trabecular and cortical bone for bone modeling and remodeling [41]. Src siRNA could enhance osteogenesis not only at trabecular surface but also the endosteal surface and intracortical surface to enhance the bone quality and decrease the bone fracture risk in the SAOP. Because of the limitation of micro-CT resolution used for the current study, we did not determine the cortical porosity of femoral neck. However it was reported that drugs with anti-resorptive effect could reduce cortical porosity [42,43], while anabolic agents could increase cortical porosity with increased cortical thickness and decreased risk of fracture because of the larger porosity of newly formed bone near the marrow cavity [44,45]. Src siRNA tested in the present study could inhibit Src activity that had dual functions, including anti-resorptive and anabolic effect that resulted in increased cortical bone quality. On the periosteal bone surface there are also abundant number of osteoblasts and preosteoclasts (mononuclear, TRAP+) responsible for cortical bone remodeling [46] and this suggested that knockdown Src in these cells would also have anti-resorptive and anabolic effect to increase periosteal diameter. However, due to limitation of micro-CT resolution and also variations in animal or bone size, the current cross-sectional study (group comparison) did not shown statistical difference in cortical periosteal (Ps.Dm) or endosteal diameter (Es.Dm). Longitudinal study (monitoring changes of bone size of same animal) with 'nano-scale' 3D analysis is desirable in future study for studying the biological and therapeutic effects of our designed Src siRNA on bone remodeling at cortical bone. As the current study was related to a local injection, the Src inhibition effects were expected to show mainly in the bone marrow and endosteal surface. Future study would focus on R&D of a systemic administration of Src siRNA for its knockdown efficiency on cortical bone, especially the periosteal region.

As this is a very first study for exploring the therapeutic effect of Src siRNA for SAOP, local injection to the target organ or tissue is expected much more efficient, *e.g.* lower dose could already achieve therapeutic effect, such as in our current proof-of-concept study for a high risk skeletal site of osteoporosis and osteoporotic fracture as compared to the systemic administration with rather lower treatment efficiency. *In vivo* distribution of Src siRNA demonstrated that 24 h after injection the

most of the injected siRNA was retained at the injection site, and a small part of siRNA that did not transfect into the local injected site was catabolized by liver and excreted to gallbladder (Supplemental Fig. S2). However, concerning clinical application, future studies may focus on R&D of systemic bone-targeting delivery system for Src siRNA to treat systemic SAOP [47,48].

In conclusion, we found corticosteroid-associated osteoporosis in an established rabbit SAON model and the knockdown of Src by Src siRNA could increase bone formation and decrease bone resorption and therefore could become a potential novel therapeutic strategy to prevent corticosteroid-associated secondary osteoporosis.

Supplementary data to this article can be found online at http://dx.doi.org/10.1016/j.bone.2015.11.010.

Conflicts of interest

All authors declare no conflict of interest in the present study.

Acknowledgments

This work was supported by the Hong Kong General Research Fund (GRF CUHK-473011), the National Natural Science Foundation of China (NSFC-81171771) and the Natural Science Foundation (NSFC-GJHS20120702084840608).

References

[1] B. Gudbjornsson, U.I. Juliusson, F.V. Gudjonsson, Prevalence of long term steroid treatment and the frequency of decision making to prevent steroid induced osteoporosis in daily clinical practice, Ann. Rheum. Dis. 61 (2002) 32–36.
[2] X.H. Xie, X.L. Wang, H.L. Yang, D.W. Zhao, L. Qin, Steroid-associated osteonecrosis: epidemiology, pathophysiology, animal model, prevention, and potential treatments (an overview), J. Orthop. Translat. 3 (2015) 58–70.
[3] J.A. Kanis, H. Johansson, A. Oden, O. Johnell, C. de Laet, L.J. Melton, et al., A meta-analysis of prior corticosteroid use and fracture risk, J. Bone Miner. Res. 19 (2004) 893–899.
[4] Y. Assouline-Dayan, C. Chang, A. Greenspan, Y. Shoenfeld, M.E. Gershwin, Pathogenesis and natural history of osteonecrosis, Semin. Arthritis Rheum. 32 (2002) 94–124.
[5] A.M. Parfitt, Osteonal and hemi-osteonal remodeling — the spatial and temporal framework for signal traffic in adult human bone, J. Cell. Biochem. 55 (1994) 273–286.
[6] R.S. Weinstein, Glucocorticoid-induced osteoporosis and osteonecrosis, Endocrinol. Metab. Clin. N. Am. 41 (2012) 595–611.
[7] T.J. Yeatman, A renaissance for SRC, Nat. Rev. Cancer 4 (2004) 470–480.
[8] N. Rucci, M. Susa, A. Teti, Inhibition of protein kinase c-Src as a therapeutic approach for cancer and bone metastases, Anti Cancer Agents Med. Chem. 8 (2008) 342–349.
[9] B. Peruzzi, A. Cappariello, A. Del Fattore, N. Rucci, F. De Benedetti, A. Teti, c-Src and IL-6 inhibit osteoblast differentiation and integrate IGFBP5 signalling, Nat. Commun. 3 (2012) 630.
[10] M. Marzia, N.A. Sims, S. Voit, S. Migliaccio, A. Taranta, S. Bernardini, et al., Decreased c-Src expression enhances osteoblast differentiation and bone formation, J. Cell Biol. 151 (2000) 311–320.
[11] T. Miyazaki, A. Sanjay, L. Neff, S. Tanaka, W.C. Horne, R. Baron, Src kinase activity is essential for osteoclast function, J. Biol. Chem. 279 (2004) 17660–17666.
[12] O. Destaing, A. Sanjay, C. Itzstein, W.C. Horne, D. Toomre, P. De Camilli, et al., The tyrosine kinase activity of c-Src regulates actin dynamics and organization of podosomes in osteoclasts, Mol. Biol. Cell 19 (2008) 394–404.
[13] P.L. Schwartzberg, L. Xing, O. Hoffmann, C.A. Lowell, L. Garrett, B.F. Boyce, et al., Rescue of osteoclast function by transgenic expression of kinase-deficient Src in src−/− mutant mice, Genes Dev. 11 (1997) 2835–2844.
[14] L.Z. Zheng, H.J. Cao, S.H. Chen, T. Tang, W.M. Fu, L. Huang, et al., Blockage of Src by specific siRNA as a novel therapeutic strategy to prevent destructive repair in steroid-associated osteonecrosis in rabbits, J. Bone Miner. Res. (2015).
[15] L. Qin, G. Zhang, H. Sheng, K.W. Yeung, H.Y. Yeung, C.W. Chan, et al., Multiple bioimaging modalities in evaluation of an experimental osteonecrosis induced by a combination of lipopolysaccharide and methylprednisolone, Bone 39 (2006) 863–871.
[16] M.L. Bouxsein, S.K. Boyd, B.A. Christiansen, R.E. Guldberg, K.J. Jepsen, R. Muller, Guidelines for assessment of bone microstructure in rodents using micro-computed tomography, J. Bone Miner. Res. 25 (2010) 1468–1486.
[17] H.R. Buie, G.M. Campbell, R.J. Klinck, J.A. MacNeil, S.K. Boyd, Automatic segmentation of cortical and trabecular compartments based on a dual threshold technique for in vivo micro-CT bone analysis, Bone 41 (2007) 505–515.
[18] D.W. Dempster, J.E. Compston, M.K. Drezner, F.H. Glorieux, J.A. Kanis, H. Malluche, et al., Standardized nomenclature, symbols, and units for bone histomorphometry: a 2012 update of the report of the ASBMR histomorphometry nomenclature committee, J. Bone Miner. Res. 28 (2013) 2–17.
[19] H. Kaji, T. Sugimoto, M. Kanatani, K. Nishiyama, K. Chihara, Dexamethasone stimulates osteoclast-like cell formation by directly acting on hemopoietic blast cells and enhances osteoclast-like cell formation stimulated by parathyroid hormone and prostaglandin E2, J. Bone Miner. Res. 12 (1997) 734–741.
[20] D. Patschan, K. Loddenkemper, F. Buttgereit, Molecular mechanisms of glucocorticoid-induced osteoporosis, Bone 29 (2001) 498–505.
[21] S.C. Manolagas, R.S. Weinstein, New developments in the pathogenesis and treatment of steroid-induced osteoporosis, J. Bone Miner. Res. 14 (1999) 1061–1066.
[22] E.M. Lau, F.W. Chan, D.S. Hui, A.K. Wu, P.C. Leung, Reduced bone mineral density in male severe acute respiratory syndrome (SARS) patients in Hong Kong, Bone 37 (2005) 420–424.
[23] J.F. Griffith, G.E. Antonio, S.M. Kumta, D.S. Hui, J.K. Wong, G.M. Joynt, et al., Osteonecrosis of hip and knee in patients with severe acute respiratory syndrome treated with steroids, Radiology 235 (2005) 168–175.
[24] M.A. Mont, L.C. Jones, T.A. Einhorn, D.S. Hungerford, A.H. Reddi, Osteonecrosis of the femoral head. Potential treatment with growth and differentiation factors, Clin. Orthop. Relat. Res. S314-35 (1998).
[25] R.S. Weinstein, Glucocorticoid-induced osteoporosis, Rev. Endocr. Metab. Disord. 2 (2001) 65–73.
[26] M. Subramaniam, D. Colvard, P.E. Keeting, K. Rasmussen, B.L. Riggs, T.C. Spelsberg, Glucocorticoid regulation of alkaline phosphatase, osteocalcin, and proto-oncogenes in normal human osteoblast-like cells, J. Cell. Biochem. 50 (1992) 411–424.
[27] T. Nishii, N. Sugano, K. Ohzono, T. Sakai, K. Haraguchi, H. Yoshikawa, Progression and cessation of collapse in osteonecrosis of the femoral head, Clin. Orthop. Relat. Res. 149-57 (2002).
[28] P. Hernigou, F. Beaujean, J.C. Lambotte, Decrease in the mesenchymal stem-cell pool in the proximal femur in corticosteroid-induced osteonecrosis, J. Bone Joint Surg. (Br.) 81 (1999) 349–355.
[29] X.H. Xie, X.L. Wang, Y.X. He, Z. Liu, H. Sheng, G. Zhang, et al., Promotion of bone repair by implantation of cryopreserved bone marrow-derived mononuclear cells in a rabbit model of steroid-associated osteonecrosis, Arthritis Rheum. 64 (2012) 1562–1571.
[30] K. Thammasitboon, S.R. Goldring, J.A. Boch, Role of macrophages in LPS-induced osteoblast and PDL cell apoptosis, Bone 38 (2006) 845–852.
[31] C. Guo, L. Yuan, J.G. Wang, F. Wang, X.K. Yang, F.H. Zhang, et al., Lipopolysaccharide (LPS) induces the apoptosis and inhibits osteoblast differentiation through JNK pathway in MC3T3-E1 cells, Inflammation 37 (2014) 621–631.
[32] G.Q. Hou, C. Guo, G.H. Song, N. Fang, W.J. Fan, X.D. Chen, et al., Lipopolysaccharide (LPS) promotes osteoclast differentiation and activation by enhancing the MAPK pathway and COX-2 expression in RAW264.7 cells, Int. J. Mol. Med. 32 (2013) 503–510.
[33] M.J. Smolinska, N.J. Horwood, T.H. Page, T. Smallie, B.M. Foxwell, Chemical inhibition of Src family kinases affects major LPS-activated pathways in primary human macrophages, Mol. Immunol. 45 (2008) 990–1000.
[34] S.K. Zaidi, A.J. Sullivan, R. Medina, Y. Ito, A.J. van Wijnen, J.L. Stein, et al., Tyrosine phosphorylation controls Runx2-mediated subnuclear targeting of YAP to repress transcription, EMBO J. 23 (2004) 790–799.
[35] P.J. Marie, Transcription factors controlling osteoblastogenesis, Arch. Biochem. Biophys. 473 (2008) 98–105.
[36] N. Furuyama, Y. Fujisawa, Regulation of collagenolytic protease secretion through c-Src in osteoclasts, Biochem. Biophys. Res. Commun. 272 (2000) 116–124.
[37] S.C. Manolagas, Birth and death of bone cells: basic regulatory mechanisms and implications for the pathogenesis and treatment of osteoporosis, Endocr. Rev. 21 (2000) 115–137.
[38] J.A. Kanis, J.D. Adachi, C. Cooper, P. Clark, S.R. Cummings, M. Diaz-Curiel, et al., Standardising the descriptive epidemiology of osteoporosis: recommendations from the epidemiology and quality of life working group of IOF, Osteoporos. Int. 24 (2013) 2763–2764.
[39] A.W. Popp, M. Windolf, C. Senn, A. Tami, R.G. Richards, S. Brianza, et al., Prediction of bone strength at the distal tibia by HR-pQCT and DXA, Bone 50 (2012) 296–300.
[40] R.M. Zebaze, A. Ghasem-Zadeh, A. Bohte, S. Iuliano-Burns, M. Mirams, R.I. Price, et al., Intracortical remodelling and porosity in the distal radius and post-mortem femurs of women: a cross-sectional study, Lancet 375 (2010) 1729–1736.
[41] U.I. Modder, S. Khosla, Skeletal stem/osteoprogenitor cells: current concepts, alternate hypotheses, and relationship to the bone remodeling compartment, J. Cell. Biochem. 103 (2008) 393–400.
[42] R.M. Zebaze, C. Libanati, M. Austin, A. Ghasem-Zadeh, D.A. Hanley, J.R. Zanchetta, et al., Differing effects of denosumab and alendronate on cortical and trabecular bone, Bone 59 (2014) 173–179.
[43] E. Seeman, P.D. Delmas, D.A. Hanley, D. Sellmeyer, A.M. Cheung, E. Shane, et al., Microarchitectural deterioration of cortical and trabecular bone: differing effects of denosumab and alendronate, J. Bone Miner. Res. 25 (2010) 1886–1894.
[44] T. Hirano, D.B. Burr, C.H. Turner, M. Sato, R.L. Cain, J.M. Hock, Anabolic effects of human biosynthetic parathyroid hormone fragment (1–34), LY333334, on remodeling and mechanical properties of cortical bone in rabbits, J. Bone Miner. Res. 14 (1999) 536–545.
[45] M. Sato, M. Westmore, A. Schmidt, Q.Q. Zeng, E.V. Glass, J. Vahle, et al., Teriparatide [PTH(1-34)] strengthens the proximal femur of ovariectomized nonhuman primates despite increasing porosity, J. Bone Miner. Res. 19 (2004) 623–629.
[46] H. Xie, Z. Cui, L. Wang, Z.Y. Xia, Y. Hu, L.L. Xian, et al., PDGF-BB secreted by preosteoclasts induces angiogenesis during coupling with osteogenesis, Nat. Med. 20 (2014) 1270–1278.
[47] X.L. Wang, Y.X. Lai, H.H. Ng, Z. Yang, L. Qin, Systemic drug delivery systems for bone tissue regeneration- a mini review, Curr. Pharm. Des. 21 (2015) 1575–1583.
[48] G. Zhang, B. Guo, H. Wu, T. Tang, B.T. Zhang, L. Zheng, et al., A delivery system targeting bone formation surfaces to facilitate RNAi-based anabolic therapy, Nat. Med. 18 (2012) 307–314.